Calculation of Vibrational Transition Frequencies and Intensities in Water Dimer: Comparison of Different Vibrational Approaches

Henrik G. Kjaergaard* and Anna L. Garden

Department of Chemistry, University of Otago, P.O. Box 56, Dunedin 9054, New Zealand and The Lundbeck Foundation Center for Theoretical Chemistry, Department of Chemistry, Aarhus University, DK-8000, Aarhus C, Denmark

Galina M. Chaban

NASA Ames Research Center, Mail Stop T27B-1, Moffett Field, California 94035-1000

R. Benny Gerber

Department of Chemistry, University of California, Irvine, California 92697 and Department of Physical Chemistry and The Fritz Haber Research Center, The Hebrew University, Jerusalem 91904, Israel

Devin A. Matthews and John F. Stanton

Center for Theoretical Chemistry, Departments of Chemistry and Biochemistry, The University of Texas at Austin, Austin, Texas 78712

Received: October 16, 2007; In Final Form: February 19, 2008

We have calculated frequencies and intensities of fundamental and overtone vibrational transitions in water and water dimer with use of different vibrational methods. We have compared results obtained with correlation-corrected vibrational self-consistent-field theory and vibrational second-order perturbation theory both using normal modes and finally with a harmonically coupled anharmonic oscillator local mode model including OH-stretching and HOH-bending local modes. The coupled cluster with singles, doubles, and perturbative triples ab initio method with augmented correlation-consistent triple-ζ Dunning and atomic natural orbital basis sets has been used to obtain the necessary potential energy and dipole moment surfaces. We identify the strengths and weaknesses of these different vibrational approaches and compare our results to the available experimental results.

Introduction

The formation of complexes gives rise to intermolecular interactions that can alter the spectroscopy of the monomeric constituents.[1−6] The hydrogen-bonded water dimer ($H_2O{\cdot}H_2O$) is the simplest water complex and knowledge of its vibrational spectrum is essential in predicting the effect water dimer has on, for example, the absorption of solar radiation.[7−10] However, the vibrational spectrum of water dimer has proven difficult to measure at ambient temperatures due to the low abundance of water dimer and the strong overlap with water monomer transitions.

Vibrational spectra of water dimer have been recorded in cold environments such as matrix isolation and jet expansion experiments, where the cluster formation can be favored.[4,11−18] The jet-cooled spectra are sometimes complicated by formation of larger clusters, and in matrix isolation spectra the vibrational transitions are perturbed by the matrix. Rotational structure has been observed for only two vibrational transitions and assignment of vibrational transitions in water dimer has been difficult.[11,14] In the matrix isolation experiments, relative vibrational intensities have been determined and absolute intensities of the four fundamental OH-stretching transitions have been measured in a recent He-droplet experiment.[15−18]

A small number of water dimer spectra have been extracted from water vapor spectra recorded at ambient temperature.[10,19−22] The laboratory spectra show broad features in which it is difficult to assign specific transitions[10,19,20] and the validity of the atmospheric observation has been questioned.[21−24]

The water dimer has twelve vibrational degrees of freedom, six attributable to the intramolecular modes of the two water molecules and six arising from the low-frequency intermolecular modes. These lower frequency modes have been successfully modeled by a semiempirical six dimensional vibration−rotation−tunneling (VRT) potential and the associated Hamiltonian models[25−28] and recently with an ab initio model that calculated a full six dimensional intermolecular potential energy surface with no fitting to experimental data.[29] An exact solution of the twelve dimensional problem is not presently possible and one has to use approximations. The different vibrational models all employ different approximations, which lead to different strengths and weaknesses. The most simple vibrational method is the double harmonic approximation, which is implemented in most current quantum chemistry programs. In this approximation, the potential is harmonic and the dipole moment linear in normal coordinates. This method is relatively fast and usually gives a reasonable idea of the fundamental vibrational

* To whom correspondence should be addressed. E-mail: henrik@chemistry.otago.ac.nz. Fax: 64-3-479-7906. Phone: 64-3-479-5378.

10.1021/jp710066f CCC: $40.75
Published on Web 04/12/2008

frequencies and intensities. There have been several double harmonic calculations of the fundamental water dimer transitions.[30−32] However, this approach cannot describe combination and overtone transitions and furthermore anharmonic corrections to energies and deviations from nonlinear dipole moment functions are often important even for fundamental transitions.[33−39]

In this work, we calculate frequencies and intensities of vibrational transitions in water and water dimer with different vibrational methods that extend beyond the double harmonic approach. We will compare three different approaches, two that add anharmonic corrections to the conventional normal mode approach and one that is based on a reduced Hamiltonian local mode approach in which the modes are inherently anharmonic.

The first approach is to include mechanical anharmonicity via standard Rayleigh−Schrödinger vibrational second-order perturbation theory (VPT2).[40] In the standard second-order perturbation theory approach, the 1D vibrational problem leads to the exact energy levels for a Morse potential. Accordingly, VPT2 is good for the stretching energy levels of polyatomic molecules in the absence of strong resonances.[41] Inclusion of nonlinearity in the dipole moment function is necessary for calculation of intensities beyond the double harmonic limit and to obtain intensities we use the VPT2 formalism given recently.[41] In conjunction with a particular atomic natural orbital (ANO) basis set, the VPT2 method has also been found empirically to work well for bending and lower frequency modes, again subject to the caveat regarding resonance.[33,41]

Second, we employ a vibrational self-consistent field (VSCF) wave function method based on the normal modes in rectilinear coordinates.[42,43] This particular vibrational wave function method is analogous to the well-known SCF method used in electronic structure theory. The method allows computation of both 1D anharmonic corrections and couplings between vibrational normal modes. There have been several ab initio VSCF algorithms developed in the recent years.[44−46] These utilize a grid representation and hence do not require fitting of potential energy surfaces. We have used the ab initio VSCF method and its correlation-corrected extension via second-order perturbation theory.[47] This can be thought of as a vibrational analogue of the MP2 electronic structure method and is also referred to as vibrational MP2 (VMP2) or correlation-corrected VSCF (cc-VSCF).[48] The cc-VSCF approach, in conjunction with the MP2 and CCSD(T) electronic structure methods, has been shown to provide reliable anharmonic vibrational frequencies for many hydrogen-bonded systems, such as water clusters and complexes of negative and positive ions with water,[49,50] complexes of inorganic acids with water,[51−54] and complexes of organic molecules with water.[55−57] Anharmonic frequencies of the highest frequency stretching vibrations were predicted with accuracy of 30−50 cm^{-1} compared with experiment.[49−57] Similar to the different ways in which one can include electronic correlation in electronic structure theory, it is also possible to improve the VSCF methods beyond the cc-VSCF approach utilized here.[48]

Alternatively to the normal mode descriptions, molecular vibration can also be described in terms of local modes, which have been used successfully to explain XH-stretching (where X is a heavier atom such as C, N, O) overtone spectra.[58−60] These local modes are inherently anharmonic, most commonly described by Morse oscillators, and coupling between them is introduced explicitly via the vibrational Hamiltonian. The high-frequency XH-stretching modes are adiabatically separated from the low-frequency modes and are harmonically coupled to one another. This comprises the so-called harmonically coupled anharmonic oscillator (HCAO) local mode model. The spectra of water and water dimer are dominated by OH-stretching and HOH-bending vibrations. These transitions have in the past been successfully modeled with the HCAO local mode model.[5,10,15−20,61,62] The HCAO local mode model clearly lacks inclusion of the lower frequency modes. However, these lower frequency modes are not likely to contribute significantly to the overall intensity of the dominant OH-stretching and HOH-bending regions transitions. The lower frequency modes could contribute to the overall band shape, as observed previously in CH-stretching overtone spectra of methyl groups with relatively free internal rotation.[63]

The current paper is split into three parts. In the first part, we compare VPT2, VSCF, cc-VSCF, and HCAO calculated frequencies and intensities of vibrational transitions of water with experimental results. We identify the strengths and weaknesses of each of the vibrational models and obtain an estimate of the level of accuracy we can expect with these methods. In the second part, we use these methods to calculate OH-stretching and HOH-bending transitions in water dimer. The effect of the lower frequency modes are investigated indirectly by comparison of the results from the full dimensional normal mode and limited dimensional local mode model. We compare our calculated results with the avilable experimental results. The matrix isolation experiments provide the largest set of data; however, this data is perturbed by matrix effects and different matrices can lead to large differences in results as we will show. In the third part, we focus on the first OH-stretching overtone region for which both jet-cooled action and matrix isolation spectra have been recorded. We extend the VPT2 and HCAO vibrational models to account for some of the deficiencies of the standard implementation of these models by including additional coupling terms between states in the first OH-stretching overtone region.

In all calculations, we have limited ourselves to states having fewer than three quanta of excitation. To facilitate comparison between the different vibrational methods, we have used the CCSD(T)/aug-cc-pVTZ ab initio method with all vibrational models. Recently, one-dimensional (1D) calculations of one of the OH-stretching vibrations in water dimer found that the CCSD(T)/aug-cc-pVTZ ab initio method provides transition frequencies and intensities that compare well with those calculated with a larger basis set.[64]

Theory and Calculations

VPT Approach. In VPT, the potential energy and dipole moment function are expanded about the molecular equilibrium

$$\hat{V}(Q)/\mathrm{cm}^{-1} = \frac{1}{2}\sum_i \omega_i Q_i^2 + \frac{1}{6}\sum_{ijk}\phi_{ijk}Q_iQ_jQ_k + \frac{1}{24}\sum_{ijkl}\phi_{ijkl}Q_iQ_jQ_kQ_l + ... \quad (1)$$

and

$$\hat{P}(Q)^\alpha/D = \sum_i P_i^\alpha Q_i + \frac{1}{2}P_{ij}^\alpha Q_iQ_j + \frac{1}{6}P_{ijk}^\alpha Q_iQ_jQ_k + ... \quad (2)$$

where Q_i are dimensionless reduced normal coordinates and the coefficients ϕ and P^α are the derivatives of the potential (force

constants) and dipole moment function respectively, evaluated at equilibrium. In VPT2, these expansions are truncated at the second-order correction to the harmonic oscillator Hamiltonian. It should be noted that in this particular realization of perturbation theory, the Hamiltonian and dipole operators themselves contain contributions from all orders, as opposed to the more common case where the Hamiltonian has a zeroth-order part and a first-order perturbation. As a result, only a subset of the expansion coefficients contribute to VPT2.

The cubic and semidiagonal quartic force constants required for VPT2 were obtained with the MAB version of the ACESII program system, via numerical differentiation of analytical second derivatives of the CCSD(T) energy.[65,66]

Intensities of fundamental and two mode excitations were also calculated with VPT2, the details of which are given in ref 41.

VSCF. The VSCF wave function method is based on a separability approximation, where the vibrational state of the system is represented by a product of 1D wave functions[42,43]

$$Y = \prod_{j}^{N} y_j(Q_j) \tag{3}$$

where N is the number of vibrational degrees of freedom and Q_j are mass-weighted normal coordinates. The method is currently implemented in normal-mode coordinates, though in principle other coordinate systems can be used.[47] The VSCF approximation reduces the problem of solving the N-dimensional vibrational Schrödinger equation to solving N single-mode VSCF equations. The resulting VSCF solutions are further corrected for correlation effects between the vibrational modes using second-order perturbation theory (cc-VSCF).[67] A combined ab initio/cc-VSCF approach has been described in detail previously.[44,47] The method uses a pairwise approximation,[67] where the potential of the system is represented by a sum of separable (single mode) terms and pair coupling terms, neglecting interactions of tertiary coupling of normal modes and higher-order interactions

$$V(Q_1, ..., Q_N) = \sum_{j}^{N} V_j^{\mathrm{diag}}(Q_j) + \sum_{i}^{N-1}\sum_{j>i}^{N} V_{ij}^{\mathrm{coup}}(Q_i, Q_j) \tag{4}$$

Diagonal (single-mode) terms $V_j^{\mathrm{diag}}(Q_j) = V(0, ..., Q_j, ..., 0)$ and the pairwise mode−mode coupling terms $V_{ij}^{\mathrm{coup}}(Q_i, Q_j) = V(0, ..., Q_i, ..., Q_j, ..., 0) - V^{\mathrm{diag}}(Q_i) - V^{\mathrm{diag}}(Q_j)$ are calculated directly from the ab initio program on 8 point grids along each normal coordinate, and on 8×8 square grids for each pair of normal coordinates. The calculated ab initio potentials are then interpolated into 16 and 16×16 point grids and used for numerical solution of the 1D VSCF equations. Intensities calculated with the VSCF approach are based on Hartree−Fock dipole moments and are not comparable with the CCSD(T) based ones computed with other methods in this study. The VSCF intensities are given in the Supporting Information.

We note that the implementation of VSCF in normal coordinates is perhaps inappropriate for certain low-frequency modes, such as soft torsional and bending modes.[47] This is due to the "grid" approach used in which the normal mode obtained about equilibrium does not describe the motion correctly for grid points far from equilibrium. Recently, a VSCF approach based on internal coordinates has been implemented that addresses this problem.[68] Also, cc-VSCF does not address resonance effects or near degeneracies. An alternative model is the use of a degenerate VSCF model such as VCI or VSCF-DPT2.[69]

HCAO Local Mode Approach. We have used a 3D harmonically coupled anharmonic oscillator (HCAO) local mode model to describe the vibrations in water.[62] For water dimer, OH-stretching and HOH-bending vibrations of each of the water units (one symmetric, proton acceptor unit and one asymmetric, proton donor unit) are treated with the same model.[61] Previously, the HCAO local mode model combined with a semiemperical potential (ab initio calculated potential parameters scaled to water) and an ab initio dipole moment function[5,61] has shown to be in good agreement with the observed OH-stretching vibrational band positions and intensities.[4,11,15,16] In this study, we use potential and dipole moment parameters directly from the electronic structure calculation without any empirical scaling.

The zeroth-order Hamiltonian is given by

$$\begin{aligned}(H - E_{|00\rangle|0\rangle})/hc = \\ v_1\tilde{\omega}_1 - (v_1^2 + v_1)\tilde{\omega}_1 x_1 + v_1\tilde{\omega}_2 - (v_2^2 + v_2)\tilde{\omega}_2 x_2 \\ + v_3\tilde{\omega}_3 - (v_3{}^2 + v_3)\tilde{\omega}_3 x_3\end{aligned} \tag{5}$$

where each local mode is described by an isolated Morse oscillator. The local mode parameters $\tilde{\omega}$ and $\tilde{\omega}x$ are determined using the ab initio calculated second-, third- and fourth-order force constants. This has been shown to produce accurate OH-stretching local mode parameters.[70] The force constants are determined from a 1D potential energy curve (grid) along the OH bond or HOH angle. The grid points are calculated for displacements from equilibrium from −0.2 to 0.2 Å in steps of 0.05 Å for OH-stretching modes and from −20 to 20° in steps of 5° for HOH-bending modes.[5,34,70]

The coupling between the two OH oscillators in each of the water units is limited to the harmonic coupling within a given vibrational manifold and gives rise to the perturbation[34]

$$H^1/hc = -\gamma'_{12}(a_1 a_2^\dagger + a_1^\dagger a_2) \tag{6}$$

where $a^\dagger$ and a are the usual ladder operators. The effective coupling coefficient γ'_{12} includes both kinetic (γ_{12}) and potential (ϕ_{12}) energy contriubtions[34]

$$\gamma'_{12} = (\gamma_{12} - \phi_{12})\sqrt{\tilde{\omega}_1\tilde{\omega}_2} = \left(\frac{-g_{12}}{2\sqrt{g_{11}g_{22}}} - \frac{f_{12}}{2\sqrt{f_{11}f_{22}}}\right)\sqrt{\tilde{\omega}_1\tilde{\omega}_2} \tag{7}$$

The kinetic energy coupling term is dependent on Wilson's g-matrix elements and is determined from the ab initio calculated optimized geometry.[71] The potential energy coupling term contains the second-order diagonal force constants (f_{11} and f_{22}) calculated from the 1D potential energy curves and the second-order off-diagonal force constant (f_{12}) calculated from 2D potential energy curves.[34]

We include Fermi coupling between the bending mode and each of the two stretching modes as

$$H^2/hc = \sum_{i=1}^{2} fr'_i(a_i a_3^\dagger a_3^\dagger + a_i^\dagger a_3 a_3) \tag{8}$$

with the Fermi resonance coupling coefficients given by[62]

$$fr'_i = \left[\left(\frac{\partial g_{33}}{\partial q_i}\right)_e \left(\frac{-q_{ci}p_{c3}^2}{4\sqrt{2}}\right) + \left(\frac{\partial g_{i3}}{\partial q_3}\right)_e \left(\frac{p_{ci}q_{c3}p_{c3}^2}{2\sqrt{2}}\right) + f_{i33}\left(\frac{q_{ci}q_{c3}^2}{4\sqrt{2}}\right)\right]\frac{1}{hc} \quad (9)$$

Similar to the harmonic coupling constant, fr' contains both kinetic energy coupling via the derivatives of Wilson's g-matrix elements and potential energy coupling by way of the third-order off-diagonal force constant (f_{i33}). The off-diagonal force constants required for the coupling constants γ' and fr' are calculated from 2D potential energy curves of the same step size as for the diagonal curves. The HCAO method utilizes curvilinear coordinates with no Eckart correction. The Eckart correction is expected to be small in water dimer.[62]

We have used both normal mode notation corresponding to the transitions calculated using the normal mode methods and local mode notation for the HCAO calculated transitions. For the proton acceptor unit the local mode notation is $|ij\rangle_{\pm}|k\rangle$ where i and j refer to the OH-stretching quanta and k refers to the HOH-bending quanta. To understand this notation in regard to normal modes it should be noted that the $\nu_1 + \nu_3$ and $2\nu_1$ normal modes approximately correlate to the $|20\rangle_-|0\rangle$ and $|20\rangle_+|0\rangle$ local modes, respectively. For the proton donor unit, we use the notation $|m\rangle_f|n\rangle_b|l\rangle$ to denote the quanta in the free and bound OH-stretching, and HOH-bending local modes, respectively.

Ab initio Details. We have used the coupled cluster including singles, doubles, and perturbative triples [CCSD(T)][72,73] method with an augmented correlation-consistent triple-ζ (aug-cc-pVTZ)[74] or an atomic natural orbital (ANO)[75] basis set in all ab initio calculations of potential energy and dipole moment surfaces. The ANO basis set has [4s2p1d] functions on H atoms and [4s3p2d1f] functions on the O atoms and is given in full in the Supporting Information. All calculations assume a frozen core [1s electrons on O].

Ab initio VSCF and cc-VSCF calculations in this study were performed using the electronic structure package GAMESS.[76,77] The default convergence thresholds were used. These calculations were based on optimized structures obtained using Gaussian03.[78]

The VPT2 calculations were performed with ACESII,[79] using numerical differentiation of analytic second energy derivatives[65] to obtain cubic and quartic force constants and numerical differentiation of analytical dipole moment derivatives to obtain second- and third-order derivatives in the dipole moment expansion. Tight cutoffs were used in the solution of unperturbed and perturbed coupled cluster equations (10^{-10}) for all amplitudes and a stepsize in dimensionless normal coordinates of 0.05. Numerical checks suggest that the quartic constants, which are the most numerically uncertain quantities involved in the calculations, are precise to within 2 cm^{-1}.

The HCAO ab initio calculations were performed with the use of MOLPRO 2002.6.[80] The convergence criteria in the geometry optimization were set to the following: gradient = 0.15×10^{-4} au, stepsize = 0.6×10^{-4} au, rms of stepsize = 0.4×10^{-4}, rms of gradient = 0.1×10^{-4}, and energy = 1×10^{-6} au. In the single point energy calculations, the convergence was set to 1×10^{-9} au. The dipole moments were calculated as first-derivatives of the energy with respect to an applied finite field. The field strength used was 0.025 au.

Results and Discussion

We have optimized the structure of water and water dimer with the CCSD(T)/aug-cc-pVTZ method using MOLPRO, Gaussian03, and ACESII and found them to be in agreement with each other and the experimental structures for water and water dimer.[81] The structure of water dimer is shown in Figure 1.

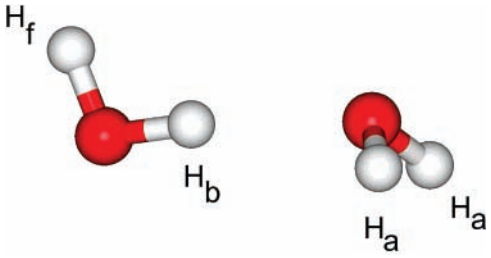

Figure 1. CCSD(T)/aug-cc-pVTZ optimized structure of water dimer.

TABLE 1: Calculated Frequencies (in cm^{-1}) of OH-Stretching Transitions in Water[a]

local mode	normal mode[b]	harmonic	VPT2	VSCF	cc-VSCF	HCAO	expt[c]
$\|10\rangle_+\|0\rangle$	100	3811	3638	3695	3627	3660	3657.1
$\|10\rangle_-\|0\rangle$	001	3920	3733	3741	3703	3759	3755.9
$\|20\rangle_+\|0\rangle$	200	7622	7193	7307	7174	7213	7201.5
$\|20\rangle_-\|0\rangle$	101	7731	7209	7404	7159	7260	7249.8
$\|11\rangle\|0\rangle$	002	7840	7371	7323	7281	7466	7445.0
$\|30\rangle_+\|0\rangle$	300	11432	10663	10834	10644	10631	10599.7
$\|30\rangle_-\|0\rangle$	201	11542	10602	10981	10543	10646	10613.4
$\|21\rangle_+\|0\rangle$	102	11651	10685	10948	10534	10903	10868.9
$\|21\rangle_-\|0\rangle$	003	11760	10913	10706	10700	11083	11032.4

[a] Calculated with potentials obtained with the CCSD(T)/aug-cc-pVTZ ab initio method. [b]Normal mode notation in the order: symmetric stretch ν_1, bend ν_2, and asymmetric stretch ν_3. [c]From the HITRAN 2006 database.

TABLE 2: Calculated Frequencies (in cm^{-1}) of HOH-bending and Stretch−Bend Combination Transitions in Water[a]

local mode	normal mode[b]	harmonic	VPT2	VSCF	cc-VSCF	HCAO	expt[c]
$\|00\rangle\|1\rangle$	010	1646	1596	1585	1580	1642	1594.7
$\|00\rangle\|2\rangle$	020	3292	3159	3152	3137	3258	3151.6
$\|00\rangle\|3\rangle$	030	4938	4690	4702	4668	4849	4666.8
$\|10\rangle_+\|1\rangle$	110	5457	5219	5246	5219	5308	5235.0
$\|10\rangle_-\|1\rangle$	011	5566	5309	5266	5215	5401	5331.3
$\|10\rangle_+\|2\rangle$	120	7103	6767	6778	6740	6926	6775.1
$\|10\rangle_-\|2\rangle$	021	7212	6852	6777	6709	7015	6871.5
$\|20\rangle_+\|1\rangle$	210	9268	8758	8822	8673	8869	8761.6
$\|20\rangle_-\|1\rangle$	111	9377	8770			8912	8807.0
$\|11\rangle\|1\rangle$	012	9486	8927	8767	8639	9109	9000.1

[a] Calculated with potentials obtained with the CCSD(T)/aug-cc-pVTZ ab initio method. [b]Normal mode notation in the order; symmetric stretch ν_1, bend ν_2, and asymmetric stretch ν_3. [c]From the HITRAN 2006 database.

Water Frequencies. In Tables 1−4, we list frequencies and intensities of vibrational transitions in water calculated with the VPT2, VSCF, cc-VSCF, and HCAO approaches. The fundamental frequencies $|10\rangle_+|0\rangle$, $|00\rangle|1\rangle$ and $|10\rangle_-|0\rangle$ are calculated to be within 50 cm^{-1} of the experimental observed frequencies with all methods. It is clear that, with the aug-cc-pVTZ basis set, both normal mode (NM) based methods are a better approximation for the HOH-bending mode and the local mode (LM) method seems to describe the OH-stretching modes better. This is perhaps not that surprising as the bending mode involves significant motion of the O-atom, which is ignored in the bending local mode. Inclusion of higher-order coupling terms in the HCAO model would improve the calculated energies of the bending modes.[83] We assume that the inherent limitations of the basis set used in this study are such that comparisons with experiment are sufficient to draw conclusions on the

TABLE 3: Calculated Oscillator Strengths of OH-Stretching Transitions in Water[a]

local mode	normal mode[b]	harmonic	VPT2	HCAO	expt[c]
$\|10\rangle_+\|0\rangle$	100	6.0×10^{-7}	3.6×10^{-7}	3.5×10^{-7}	6.0×10^{-7}
$\|10\rangle_-\|0\rangle$	001	1.0×10^{-5}	9.0×10^{-6}	7.9×10^{-6}	8.7×10^{-6}
$\|20\rangle_+\|0\rangle$	200		8.3×10^{-8}	7.0×10^{-8}	9.2×10^{-8}
$\|20\rangle_-\|0\rangle$	101		6.1×10^{-7}	5.8×10^{-7}	6.1×10^{-7}
$\|11\rangle\|0\rangle$	002		1.7×10^{-9}	3.7×10^{-9}	4.9×10^{-9}
$\|30\rangle_+\|0\rangle$	300		1.6×10^{-9}	6.2×10^{-10}	1.9×10^{-9}
$\|30\rangle_-\|0\rangle$	201		1.5×10^{-8}	1.6×10^{-8}	2.1×10^{-8}
$\|21\rangle_+\|0\rangle$	102		5.6×10^{-12}	6.3×10^{-10}	6.9×10^{-10}
$\|21\rangle_-\|0\rangle$	003		1.0×10^{-8}	3.2×10^{-9}	2.4×10^{-9}

[a] Calculated with potentials and dipole moments obtained with the CCSD(T)/aug-cc-pVTZ ab initio method. Oscillator strengths can be converted to integrated absorbance in km/mol by multiplication by 5.3313×10^6. [b] Normal mode notation in the order; symmetric stretch ν_1, bend ν_2, and asymmetric stretch ν_3. [c] From the HITRAN 2006 database.

TABLE 4: Calculated Oscillator Strengths of HOH-bending and Stretch−Bend Combination Transitions in Water[a]

local mode	normal mode[b]	harmonic	VPT2	HCAO	expt[c]
$\|00\rangle\|1\rangle$	010	1.3×10^{-5}	1.3×10^{-5}	1.3×10^{-5}	1.2×10^{-5}
$\|00\rangle\|2\rangle$	020		9.8×10^{-8}	2.1×10^{-8}	9.3×10^{-8}
$\|00\rangle\|3\rangle$	030		1.0×10^{-9}	3.6×10^{-11}	4.4×10^{-10}
$\|10\rangle_+\|1\rangle$	110		1.4×10^{-8}	1.7×10^{-8}	4.3×10^{-8}
$\|10\rangle_-\|1\rangle$	011		7.2×10^{-7}	9.4×10^{-7}	9.4×10^{-7}
$\|10\rangle_+\|2\rangle$	120		2.4×10^{-9}	2.2×10^{-9}	3.3×10^{-9}
$\|10\rangle_-\|2\rangle$	021		4.7×10^{-8}	1.3×10^{-8}	5.0×10^{-8}
$\|20\rangle_+\|1\rangle$	210		7.1×10^{-10}	6.4×10^{-10}	1.6×10^{-9}
$\|20\rangle_-\|1\rangle$	111		2.1×10^{-8}	2.0×10^{-8}	3.9×10^{-8}
$\|11\rangle\|1\rangle$	012		1.9×10^{-10}	1.5×10^{-10}	8.1×10^{-10}

[a] Calculated with potentials and dipole moments obtained with the CCSD(T)/aug-cc-pVTZ ab initio method. Oscillator strengths can be converted to integrated absorbance in km/mol by multiplication by 5.3313×10^6. [b] Normal mode notation in the order; symmetric stretch ν_1, bend ν_2, and asymmetric stretch ν_3. [c] From the HITRAN 2006 database.

relative merits of each method. However, the ultimate test of the method is a comparison with either exact variational results obtained with the same (CCSD(T)/aug-cc-pVTZ) potential energy surface or comparison with experiment in the limit of an electronic structure treatment equivalent to full configuration interaction and a complete basis set. However, for reasons mentioned in ref 82, the first comparison is even, in principle, problematic, and the second is clearly impossible given the size of the system.

For stretching overtone and combination modes, the observations for the fundamental transitions are accentuated. The LM approach is particularly good for the $|v0\rangle_\pm$ modes, the pure local mode states, which are usually the stronger transitions and the transitions on which the LM model is based.

In the vibrational wavefunction methods, there are surprisingly large discrepancies between the VSCF and the cc-VSCF methods for the stretching states. This usually indicates that the perturbation is not converged at second-order and the calculated frequencies are suspicious. These transitions may be affected by near-degeneracies. The cc-VSCF method is a nondegenerate perturbation theory treatment of VSCF and as such the perturbation series may converge more slowly. An example of such a state in this study is the $|20\rangle_-|0\rangle$ state which goes from 7404 to 7159 cm^{-1} indicating a significant perturbation. This issue seems to be more significant the higher the energy. We note that the perturbation is correcting the energy in the right direction but by considerably too much. This is in line with the usual behavior of second-order perturbation theory, which tends to overshoot when the correction is large. This indicates a problem with the cc-VSCF results for these particular states. In a recent similar calculation, large variation between the VSCF and VCI results were also observed. For example, the calculated energy of the $|11\rangle|0\rangle$ state was found to differ $\sim$400 cm^{-1} between the VSCF and VCI result with the VCI in much better agreement with experiment.[84]

The frequencies of the bending fundamental and first overtone are predicted well by both cc-VSCF and VPT2 methods, whereas the HCAO frequencies are significantly higher than experiment. Limited variation is found between the VSCF and cc-VSCF results, and the previous VSCF/VCI results.[84] The same is true for the stretch−bend combination states $|10\rangle_\pm|1\rangle$ and $|10\rangle_\pm|2\rangle$ with the HCAO results differing from experiment by up to 100 cm^{-1}.

Water Intensities. Intensities have only been calculated with the VPT2 and HCAO methods. The calculated intensities of the fundamental transitions are very similar for the two methods, despite these two methods using a normal and local mode basis, respectively. This is especially true for the symmetric states which are less affected by Eckart rotation of the frame, which is inherent in the VPT2 calculation but not included in the HCAO calculation. Eckart correction of the asymmetric fundamental was previously found to increase the intensity by $\sim$25%, which in the present calculation would bring it very close to the VPT2 result.[62] The VPT2 method predicts the intensity for the first bending overtone very well, but both VPT2 and HCAO methods predict much stonger and weaker intensities, respectively, than experiment for the second bending overtone. The previous VSCF and VCI calculation predicts intensities similar to the present VPT2 results for the fundamental vibrations and first bending overtone.[84] It is interesting that the present calculations as well as the recent VCI calculation all predict very similar intensity of the $|10\rangle_+|0\rangle$ transition, and all about a factor of 2 lower than experiment.

For the first OH-stretching overtone transitions, both methods predict the intensities of the pure OH-stretching modes quite well, but for the weakest transition, $|11\rangle|0\rangle$, the VPT2 method predicts an intensity less than half the experimental value. For the second OH-stretching overtone transitions, the discrepancies are slightly larger as expected but in general are still reasonable. The exception is the VPT2 predictions for the $|21\rangle_+|0\rangle$ transition which is 2 orders of magnitude smaller than the experimental result.

As expected from the good description of the fundamental and first overtone bending intensities obtained with the VPT2 method, it also predicts the stretch−bend combination modes accurately. The HCAO approach also does reasonably well, and for some transitions, the VPT2 method is closer to experiment (for example the $|10\rangle_\pm|2\rangle$ state) and for some the HCAO method is closer ($|10\rangle_\pm|1\rangle$). The $|11\rangle|1\rangle$ intensity is not predicted well by the HCAO method, as perhaps expected because it does not include dipole moment terms that combine all three modes.

A recent variational calculation on water with an exact kinetic energy operator showed that the maximum error in frequencies with the CCSD(T)/aug-cc-pVTZ method as compared with experiment was $\sim$50 cm^{-1} for 3 quanta excitations.[83] The VPT2 method calculated fundamental frequencies that are within 5 cm^{-1} of the variational result and for 2 quanta excitation the discrepancy increases to 40 cm^{-1}. For these lower energy transitions, VPT2 is clearly the best of the three methods. For higher energy transitions, the errors start to increase. For the pure OH-stretching transitions the HCAO method does better

TABLE 5: Calculated Frequencies (in cm^{-1}) of Fundamental Transitions in Water Dimer[a]

local mode	normal mode[b]	harmonic[c]	VPT2	VSCF	cc-VSCF	HCAO	expt
$\|0\rangle_f\|1\rangle_b\|0\rangle$	ν_3/ν_1 (d)	3731	3591	3508	3499	3565	3601[d]
$\|1\rangle_f\|0\rangle_b\|0\rangle$	ν_1/ν_3 (d)	3891	3711	3669	3665	3729	3735[d]
$\|10\rangle_+\|0\rangle$	ν_2/ν_1 (a)	3805	3634	3622	3560	3655	3660[d]
$\|10\rangle_-\|0\rangle$	ν_9/ν_3 (a)	3911	3725	3642	3608	3752	3745[e]
$\|0\rangle_f\|0\rangle_b\|1\rangle$	ν_4/ν_2 (d)	1668	1614	1615	1603	1662	1616[f]
$\|00\rangle\|1\rangle$	ν_5/ν_2 (a)	1647	1603	1583	1567	1642	1599[f]
	$\nu_{10}/\perp$ bend	622	495				523[f]
	$\nu_6/\|\|$ bend	360	304				311[f]
	ν_7/OO-str	185	144				143[g]
	ν_{11}/twist	145	122				108[h]
	ν_8/wag	154	121				103[h]
	ν_{12}/torsion	129	85				88[h]

[a] Calculated with potentials obtained with the CCSD(T)/aug-cc-pVTZ ab initio method. [b] Normal mode notation and description, with (a) and (d) indicating the corresponding water normal modes on the acceptor and donor units, respectively. The intermolecular modes are often strongly mixed. [c] Harmonic oscillator normal mode calculation. [d] From ref 89. [e] From ref 11. [f] From ref 17. [g] From ref 25. [h] From ref 90.

TABLE 6: Calculated Frequencies (in cm^{-1}) of OH-Stretching First Overtone Transitions in Water Dimer[a]

local mode	normal mode	VPT2	VSCF	cc-VSCF	HCAO	expt[b]
$\|0\rangle_f\|2\rangle_b\|0\rangle$	$2\nu_3$	7040	6896	6862	6978	7018
$\|2\rangle_f\|0\rangle_b\|0\rangle$	$\nu_1+\nu_3$	7230	7162	7025	7229	7237[c]
$\|1\rangle_f\|1\rangle_b\|0\rangle$	$2\nu_1$	7285	7206	7216	7352	7362
$\|20\rangle_+\|0\rangle$	$2\nu_2$	7186	7153	7032	7204	7207[c]
$\|20\rangle_-\|0\rangle$	$\nu_2+\nu_9$	7199	7180	6965	7250	7245[c]
$\|11\rangle\|0\rangle$	$2\nu_9$	7355	7276	7259	7452	
	$\nu_2+\nu_3$	7219	7140	7051		
	$\nu_2+\nu_1$	7343	7311	7240		
	$\nu_9+\nu_3$	7312	7157	7083		
	$\nu_9+\nu_1$	7436	7328	7271		

[a] Calculated with potentials obtained with the CCSD(T)/aug-cc-pVTZ ab initio method. [b] From Ne-matrix isolation experiments.[17] [c] The frequency of these transitions in the action spectrum of ref 14 are 7240, 7193, and 7250 cm^{-1}, respectively. The transitions observed at 7282 cm^{-1} in the action spectrum are not observed in the matrix.

TABLE 7: Calculated Frequencies (in cm^{-1}) of Stretch−Bend Combination and HOH-Bending Overtone Transitions in Water Dimer[a]

local mode	normal mode	VPT2	VSCF	cc-VSCF	HCAO	expt[b]
$\|0\rangle_f\|1\rangle_b\|1\rangle$	$\nu_3+\nu_4$	5194	5089	5035	5235	5190
	$\nu_3+\nu_5$	5193	5098	5044		
$\|1\rangle_f\|0\rangle_b\|1\rangle$	$\nu_1+\nu_4$	5309	5264	5225	5392	5333
	$\nu_1+\nu_5$	5314	5268	5228		
$\|10\rangle_+\|1\rangle$	$\nu_2+\nu_5$	5222	5174	5111	5303	5243
	$\nu_2+\nu_4$	5247	5242	5191		
$\|10\rangle_-\|1\rangle$	$\nu_9+\nu_5$	5308	5175	5126	5393	5328
	$\nu_9+\nu_4$	5338	5261	5221		
$\|0\rangle_f\|0\rangle_b\|2\rangle$	$2\nu_4$	3193	3202	3178	3295	3194
$\|00\rangle\|2\rangle$	$2\nu_5$	3177	3148	3116	3257	3163
	$\nu_4+\nu_5$	3212	3198	3175		

[a] Calculated with potentials obtained with the CCSD(T)/aug-cc-pVTZ ab initio method. [b] From Ne-matrix isolation experiments.[17]

TABLE 8: Calculated Oscillator Strengths of Fundamental Transitions in Water Dimer[a]

local mode	normal mode	harmonic[b]	VPT2	HCAO	expt[c]
$\|0\rangle_f\|1\rangle_b\|0\rangle$	ν_3	4.8×10^{-5}	2.8×10^{-5}	5.7×10^{-5}	2.5×10^{-5}
$\|1\rangle_f\|0\rangle_b\|0\rangle$	ν_1	1.9×10^{-5}	1.2×10^{-5}	1.5×10^{-5}	$\sim1.4\times10^{-5}$
$\|10\rangle_+\|0\rangle$	ν_2	1.4×10^{-6}	0.9×10^{-6}	1.8×10^{-6}	$\sim0.8\times10^{-6}$
$\|10\rangle_-\|0\rangle$	ν_9	1.4×10^{-5}	1.1×10^{-5}	1.3×10^{-5}	$\sim0.6\times10^{-5}$
$\|0\rangle_f\|0\rangle_b\|1\rangle$	ν_4	7.0×10^{-6}	0.7×10^{-5}	0.8×10^{-5}	
$\|00\rangle\|1\rangle$	ν_5	1.6×10^{-5}	1.3×10^{-5}	1.4×10^{-5}	
	ν_{10}	1.7×10^{-5}	1.4×10^{-5}		
	ν_6	9.3×10^{-6}	1.3×10^{-6}		
	ν_7	2.7×10^{-5}	1.2×10^{-5}		
	ν_{11}	7.6×10^{-6}	2.1×10^{-5}		
	ν_8	2.5×10^{-5}	3.1×10^{-5}		
	ν_{12}	2.4×10^{-5}	1.0×10^{-5}		

[a] Calculated with potentials and dipole moments obtained with the CCSD(T)/aug-cc-pVTZ ab initio method. Oscillator strengths can be converted to integrated absorbance in km/mol by multiplication by 5.3313×10^6. [b] Harmonic oscillator normal mode calculation. [c] From ref 18.

than VPT2 as the anharmonicity starts to become more important. The VSCF frequencies are worse than those calculated with the VPT2 method. The cc-VSCF frequencies are accidentally closer to the variational result however the use of nondegenerate perturbation theory make it sensitive to near degeneracies. Both VPT2 and HCAO methods predict intensities, which deviate by less than a factor of 2 from experiment for the fundamental transitions and up to a factor of 4 for the overtone transitions. The variation between the methods increases with energy and is significantly larger for states including bending motion. These results for water illustrate the accuracy we can expect for the different transitions in water dimer with these vibrational models and the CCSD(T)/aug-cc-pVTZ ab initio method. The error in the HCAO method is to some extent balanced by the error in the ab initio method as seen by comparison with the variational results.[83] This leads to reasonable agreement with experiment for the OH-stretching transitions with energies within 50 cm^{-1} and intensities within a factor of 2 for transitions up to $v = 3$.

Water Dimer Frequencies. In Tables 5−10, we present the frequencies and intensities of OH-stretching and HOH-bending transitions in water dimer. Also included are frequencies and intensities of the six intermolecular modes calculated using the double harmonic and VPT2 methods. The HCAO local mode model does not include these intermolecular modes. The VSCF method computes inaccurate values for these vibrations because of the inadequacy of the normal mode coordinate system for their proper description. Therefore, we do not include VSCF and cc-VSCF frequencies for these modes. The results in Tables 5−10 are calculated with the aug-cc-pVTZ basis set whereas VPT2 and HCAO results with the ANO basis set are given in the Supporting Information in Tables S5−S10. We have calculated the permanent dipole moment of water as a check as to whether both basis sets contain enough diffuse basis functions to describe the dipole moment function adequately. We find that the dipole moment calculated with the ANO and aug-cc-pVTZ basis sets are +0.04 and −0.02 Debye different from the experimental value, respectively.[85] This suggests that both basis sets are very well equipped to describe the dipole moment function, and hence the intensities. The experimental data for water dimer are in general much less accurate and less complete

TABLE 9: Calculated Oscillator Strengths of OH-stretching First Overtone Transitions in Water Dimer[a]

local mode	normal mode	VPT2	HCAO
$\|0\rangle_f\|2\rangle_b\|0\rangle$	$2\nu_3$	1.5×10^{-8}	1.1×10^{-8}
$\|2\rangle_f\|0\rangle_b\|0\rangle$	$\nu_1 + \nu_3$	2.2×10^{-7}	3.0×10^{-7}
$\|1\rangle_f\|1\rangle_b\|0\rangle$	$2\nu_1$	1.9×10^{-7}	6.0×10^{-8}
$\|20\rangle_+\|0\rangle$	$2\nu_2$	1.3×10^{-7}	1.2×10^{-7}
$\|20\rangle_-\|0\rangle$	$\nu_2 + \nu_9$	6.0×10^{-7}	5.7×10^{-7}
$\|11\rangle\|0\rangle$	$2\nu_9$	6.5×10^{-9}	2.9×10^{-9}
	$\nu_2 + \nu_3$	9.3×10^{-9}	
	$\nu_2 + \nu_1$	1.5×10^{-8}	
	$\nu_9 + \nu_3$	4.1×10^{-11}	
	$\nu_9 + \nu_1$	3.6×10^{-9}	

[a] Calculated with potentials and dipole moments obtained with the CCSD(T)/aug-cc-pVTZ ab initio method. Oscillator strengths can be converted to integrated absorbance in km/mol by multiplication by 5.3313×10^6.

TABLE 10: Calculated Oscillator Strengths of Stretch−Bend Combination and HOH-bending Overtone Transitions in Water Dimer[a]

local mode	normal mode	VPT2	HCAO
$\|0\rangle_f\|1\rangle_b\|1\rangle$	$\nu_3 + \nu_4$	5.3×10^{-7}	7.2×10^{-7}
	$\nu_3 + \nu_5$	2.2×10^{-8}	
$\|1\rangle_f\|0\rangle_b\|1\rangle$	$\nu_1 + \nu_4$	1.0×10^{-6}	8.6×10^{-7}
	$\nu_1 + \nu_5$	5.1×10^{-8}	
$\|10\rangle_+\|1\rangle$	$\nu_2 + \nu_5$	1.3×10^{-8}	2.5×10^{-8}
	$\nu_2 + \nu_4$	4.5×10^{-10}	
$\|10\rangle_-\|1\rangle$	$\nu_9 + \nu_5$	9.3×10^{-7}	9.6×10^{-7}
	$\nu_9 + \nu_4$	3.5×10^{-8}	
$\|0\rangle_f\|0\rangle_b\|2\rangle$	$2\nu_4$	1.1×10^{-6}	1.6×10^{-6}
$\|00\rangle\|2\rangle$	$2\nu_5$	1.4×10^{-7}	4.6×10^{-8}
	$\nu_4 + \nu_5$	4.6×10^{-8}	

[a] Calculated with potentials and dipole moments obtained with the CCSD(T)/aug-cc-pVTZ ab initio method. Oscillator strengths can be converted to integrated absorbance in km/mol by multiplication by 5.3313×10^6.

than for water. We include experimental frequencies obtained from Ne-matrix isolation and jet-cooled experiments. The jet-cooled spectra provide more accurate data and we use these where possible. Relative intensities are taken from the most recent matrix isolation experiment, apart from the fundamental OH-stretching transitions for which absolute intensities from a He-dropet experiment are used. The difference between the experimental techniques can be several cm^{-1} and transitions seen with one technique are not necessarily observed with another. For water, we found that the cc-VSCF frequencies improved the VSCF frequencies in the right direction but by too much, resulting in the experimental frequency lying somewhere between the two calculated values. For water dimer, we find that cc-VSCF is lowering the VSCF frequencies, which are already lower than the experimental values. As a consequence the cc-VSCF frequencies of the fundamental transitions differ from the experimental values by 70−140 cm^{-1}.

For the fundamental OH-stretching transitions we see that the HCAO model generally performs well with the bonded OH-stretching transition within 35 cm^{-1} of experiment and the other three transitions within 10 cm^{-1}. For the VPT2 method the agreement with experiment for the bonded OH-stretching transitions is 10 cm^{-1} and for the other OH-stretching modes within 25 cm^{-1}. Interestingly, using the ANO basis set (see Supporting Information, Table S5) the situation is reversed, with the $|0\rangle_f|1\rangle_b|0\rangle$ state being better described by the HCAO method, and the remaining OH-stretching modes better described by the VPT2 method. For the HOH-bending fundamentals we see that, again similar to water, the NM models predict the transition energy better than the LM model, with the VPT2 method agreeing with experiment to within 4 cm^{-1} with the aug-cc-pVTZ basis set and 12 cm^{-1} with the ANO basis set.

In general, the pure OH-stretching overtones are predicted well with the HCAO model compared with the Ne matrix experiments[17] and are also in good agreement with the VPT2 results. However, the inaccuracy of the OH_b-stretching frequency observed in the fundamental transition is more pronounced in the first overtone transition. The VPT2 result for the frequency of $|0\rangle_f|2\rangle_b|0\rangle$ is 20 cm^{-1} below and the HCAO results 40 cm^{-1} above the Ne matrix value. With the ANO basis set (Supporting Information, Table S6) the HCAO energy is 30 cm^{-1} higher, and VPT2 energy is 85 cm^{-1} higher than the experimental value. For the mixed OH-stretching states $|1\rangle_f|1\rangle_b|0\rangle$ and $|11\rangle|0\rangle$, the NM frequencies are significantly lower than the LM values.

We have presented four OH-stretching transitions that are combinations of OH-stretching modes located on different two water units. These transitions are neglected in the HCAO model. For the intramolecular stretch−bend combinations, we see that the VPT2 method produces the best agreement to experiment, followed by HCAO and then the VSCF methods.

Water Dimer Intensities. Experimental measurements of the intensities of water dimer transitions are scarce. In the fundamental region, we compare with the absolute He-droplet intensites and find that in general the VPT2 and HCAO intensities are similar; however, the VPT2 intensities are lower and are in very good agreement with the absolute intensities from the He droplet experiment (Table 8).[18] For all fundamental OH-stretching modes, we observe a significant increase in intensity compared with the OH-stretching transitions in water. It is interesting that for water the VPT2 and HCAO methods give almost the same intensity for the $|10\rangle_+|0\rangle$ transition, whereas for water dimer the comparable transitions ($|10\rangle_+|0\rangle$ and $|0\rangle_f|1\rangle_b|0\rangle$) are approximately half the intensity with the VPT2 method.

The intensities of the stretch−bend combination transitions are similar for the two methods with variations of less than a factor of 2 for the weak features (Table 10). For the stretch−bend combinations and the mixed OH-stretching states (Table 9), we find that transitions which are localized on one water unit are an order of magnitude stronger than those involving modes on both water units. This indicates that the basic assumption in the HCAO calculations of no interaction between the two water units is reasonable.

In the first OH-stretching overtone region, we notice a sharp decrease in intensity of the OH_b-stretching mode relative to the fundamental transition (Table 9). This is attributable to a cancellation of terms in the dipole moment expansion.[35] As a result, this state is sensitive to couplings with other modes, and we will investigate this in more detail in the next section.

In Figures 2−4, we compare relative intensities obtained from Ar and Ne matrix isolation spectra[15,17] with our calculated intensities. For each of the calculations and experiments, we have set the intensity of the fundamental OH_f-stretching transition to 100. We have chosen this transitions as reference rather than the strongest OH_b-stretching fundamental ($|0\rangle_f|1\rangle_b|0\rangle$). The OH_b-stretching mode is more sensitive to theoretical method and is also perturbed more strongly by matrix effects than the other fundamental transitions. It is clear that both VPT2 and HCAO yield relative intensities that are in good agreement with each other and with the relative intensities of the Ne and Ar matrix experiments. These intensities span more than 2 orders of magnitude. The difference between the VPT2 and HCAO

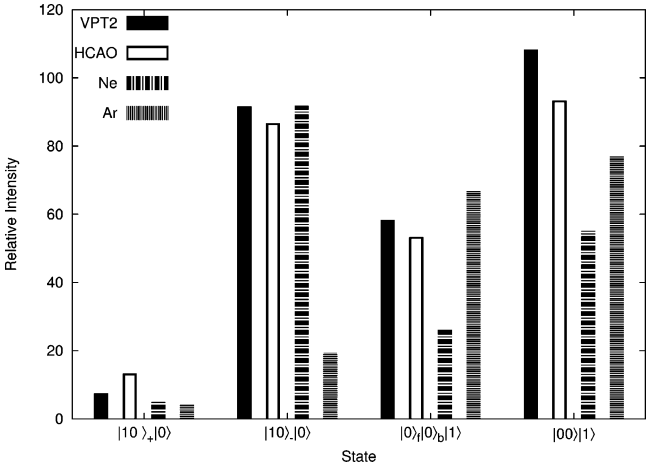

Figure 2. Relative intensities of fundamental transitions in water dimer. The intensity of $|1\rangle_f|0\rangle_b|0\rangle$ is set to 100 for each of the methods and experiments.

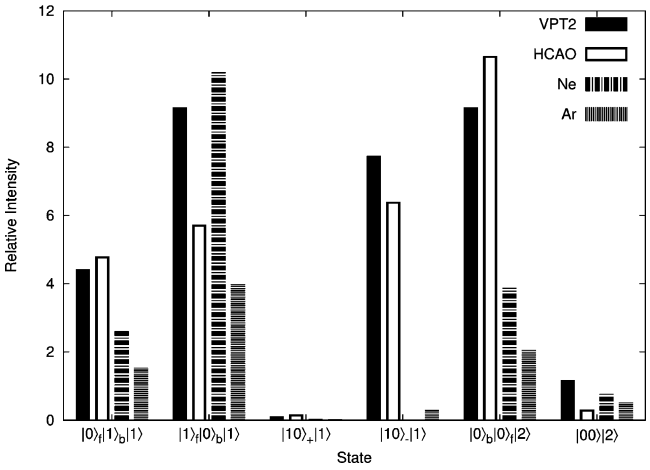

Figure 3. Relative intensities of stretch−bend combination and HOH-bending overtone transitions in water dimer. The intensity of $|1\rangle_f|0\rangle_b|0\rangle$ is set to 100 for each of the methods and experiments.

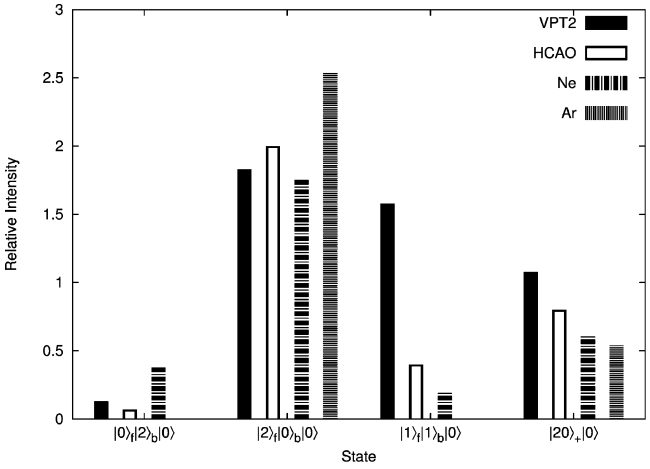

Figure 4. Relative intensities of OH-stretching overtone transitions in water dimer. The intensity of $|1\rangle_f|0\rangle_b|0\rangle$ is set to 100 for each of the methods and experiments.

intensities is in most cases less than the difference between the Ne and Ar matrix results. Intensities calculated with the ANO basis are given in the Supporting Information and yield similar agreement with experiment.

The advantage of the VPT2 method is that all 12 vibrational modes are included, whereas the advantage of the HCAO method is that anharmonic wavefunctions are inherent and that higher order dipoles are included so that higher overtone transitions can be calculated. The comparison between the two clearly shows that the effect of the six lower frequency modes on the intensity of the dominant OH-stretching is limited, and thus the previously calculated HCAO OH-stretching intensities are of reasonable accuracy.[5,61,64] The effect of the lower frequency modes is to spread the intensity and thereby change the band profile of the OH-stretching transitions.[86]

A full list of VPT2 transitions with oscillator strengths larger than 10^{-13} are given in the Supporting Information (Tables S14−S17). We find that on the high-energy side of the fundamental OH-stretching transitions there are several transitions that carry some intensity. These are combinations of the fundamental OH-stretching and low-frequency vibrations. This is in good agreement with the observed room-temperature experiments in the 3100−4400 cm^{-1} region.[20]

Largely the strengths and weakness of each method exhibited in the calculation of water are also observed for water dimer. The HCAO and VPT2 models produce the most accurate frequencies for the OH-stretching modes with an accuracy of better than 1% when compared with experiment. It is clear that the normal mode models perform better than the local mode model in describing the bending mode. This problem with the HCAO local mode model can be aleviated by improving the description of the coupling.[83] The OH_b-stretching mode is probably the most difficult mode to describe. Improving the basis set toward complete basis set limit and consideration of counterpoise correction has been shown to increase the frequency of the OH_b-stretching mode but have little effect on the intensity.[64] Thus increasing the basis set could bring the VPT2 frequencies in excellent agreement with the experimental values. The VPT2 method is the only method used that is appropriate to model the six intermolecular vibrations. The HCAO model does not include these, and the VSCF methods used in this study are inapplicable for these types of modes. In comparison to water, the water dimer fundamental transitions are stronger and the first overtone transitions are weaker. The intensities predicted using the VPT2 and HCAO methods are similar with the difference between them usually being less than between the Ne and Ar matrix isolation results. The ANO and aug-cc-pVTZ basis sets used are of similar size and give similar results. We find that the VPT2 method seems to produce the best results when paired with the ANO basis set, and the HCAO method when using the aug-cc-pVTZ basis set.

First OH-Stretching Overtone in Water Dimer. The first OH-stretching overtone region of the water dimer spectrum has been measured both with matrix isolation techniques and high-resolution jet-cooled action spectroscopy. There is limited agreement between the experimental results. Despite observation of rotational structure in a transition observed in the jet-cooled spectrum, assignment of this transition is still not clear. We have improved the VPT2 and HCAO models to try and assign this region. The first OH-stretching overtone region of water dimer is more complex than the fundamental region with the two quanta of excitation being available for distribution among the four OH-stretching modes, resulting in a total of ten possible OH-stretching states in the $v_{OH} = 2$ manifold. In a normal mode description of water, it has been shown that the so-called Darling−Dennison second-order resonance becomes important, that is, coupling states of quantum numbers (ν_1, ν_2, ν_3) and ($\nu_1 - 2$, ν_2, $\nu_3 + 2$) that have the same symmetries and similar energies.[71,87] We have extended the VPT2 method to include such resonances in the $v_{OH} = 2$ manifold. We treat this manifold

TABLE 11: Calculated Frequencies and Oscillator Strengths of the States in the $v_{OH} = 2$ Manifold[a,b]

VPT2+K			HCAO+IU		
assignment	frequency	oscillator strength	frequency	oscillator strength	assignment
a' states					
$\|0\rangle_f\|2\rangle_b$	7026	1.6×10^{-8}	6978	1.0×10^{-8}	$\|0\rangle_f\|2\rangle_b$
$\|20\rangle_+$	7132	5.1×10^{-9}	7199	6.4×10^{-8}	$\|20\rangle_+$
$\|2\rangle_f\|0\rangle_b + \|20\rangle_+$*	7162	3.8×10^{-7}	7225	6.8×10^{-8}	$\|0\rangle_f\|1\rangle_b\|10\rangle_+$*
$\|0\rangle_f\|1\rangle_b\|10\rangle_+$*	7236	1.6×10^{-7}	7228	3.0×10^{-7}	$\|2\rangle_f\|0\rangle_b$*
$\|2\rangle_f\|0\rangle_b$*	7311	1.1×10^{-8}	7351	6.3×10^{-8}	$\|1\rangle_f\|1\rangle_b$*
$\|11\rangle$	7378	5.1×10^{-9}	7385	9.1×10^{-10}	$\|1\rangle_f\|0\rangle_b\|10\rangle_+$
$\|1\rangle_f\|0\rangle_b\|10\rangle_+$*	7443	3.1×10^{-8}	7452	3.1×10^{-9}	$\|11\rangle$
a'' states					
$\|20\rangle_-$	7193	5.7×10^{-7}	7249	5.5×10^{-7}	$\|20\rangle_-$
$\|0\rangle_f\|1\rangle_b\|10\rangle_-$	7311	$< 1 \times 10^{-9}$	7317	4.3×10^{-8}	$\|0\rangle_f\|1\rangle_b\|10\rangle_-$
$\|1\rangle_f\|0\rangle_b\|10\rangle_-$	7443	3.1×10^{-8}	7481	2.6×10^{-9}	$\|1\rangle_f\|0\rangle_b\|10\rangle_-$

[a] Calculated with potentials and dipole moments obtained with the CCSD(T)/aug-cc-pVTZ ab initio method. Oscillator strengths can be converted to integrated absorbance in km/mol by multiplication by 5.3313×10^6. [b] Asterisks are used to mark states with large mixing.

with the dressed Hamiltonian approach outlined by Lehmann[88] in which the off-diagonal matrix elements coupling these states are approximated at second-order in the perturbation (consisting of a leading quartic term and a term that is bilinear in the cubic force constants) and the final levels are obtained by explicit diagonalization.[82] Eigenvectors associated with the seven states of a' and three states of a'' symmetry were then used to rotate the VPT2 transition moments to the diagonal representation, thereby affecting the intensities. This method is denoted VPT2+K and the detailed results are given in the Supporting Information in Table S11. We have also extended the HCAO model to describe all of the transitions in this manifold by including harmonic coupling between OH-stretching modes on different water units. The necessary grids are calculated similar to those for each water unit by displacing the OH bonds from -0.2 to 0.2 Å in steps of 0.1 Å. We include only harmonic coupling and assume the kinetic energy coupling between acceptor unit and the OH_f-stretching mode to be zero and negligible for the OH_b-stretching mode. We have limited the mixed interunit dipole derivatives to include only the μ_{11} term. We denote this method HCAO+IU and the detailed results are given in the Supporting Information Table S12, and in Table S13 we compare the effects of including various degrees of coupling in the HCAO model.

We adopt the local mode notation in both cases to avoid confusion regarding assignments. We are interested only in the stretching modes and therefore omit specifying the bending quanta (which is zero) for simplicity. For the proton acceptor unit, this notation is $|ij\rangle_\pm$ where i and j refer to the OH-stretching quanta; and for the proton donor unit, the notation is $|m\rangle_f|n\rangle_b$, denoting the quanta in the free and bound OH-stretching local modes. For the states consisting of transitions on different units, we use the combined notation of $|m\rangle_f|n\rangle_b|ij\rangle_\pm$.

In Table 11, we present the energies and intensities of the ten states within the first OH-stretching overtone manifold with the comparable ANO results given in the Supporting Information Tables S11 and S12. We have grouped the states according to the symmetry species of vibration to facilitate assignment. Comparison with the VPT2 and HCAO results in Tables 6 and 9 shows that overall the VPT2 calculated energies and intensities are more strongly perturbed by the inclusion of Darling−Dennison coupling than the HCAO calculated results are by the inclusion of interunit coupling.

For the three states of a'' symmetry, both methods calculate these states to be essentially "pure" in that there is minimal coupling to other states. We assign the lowest energy a'' state to the $|20\rangle_-$ state, which is predicted by both methods to be the strongest transition in the $v_{OH} = 2$ manifold. The position of the $|0\rangle_f|1\rangle_b|10\rangle_-$ state shows reasonable agreement between the two methods, whereas the agreement for the $|1\rangle_f|0\rangle_b|10\rangle_-$ state is worse with a difference in energy of around 40 cm^{-1}. We note that for these two interunit transitions the VPT2+K and HCAO+IU calculated intensities are significantly different. Overall the total intensity of the three a'' transitions is very similar with the two calculations.

For the states of a' symmetry there is a high degree of mixing and many of the eigenstates are combinations of several different states, to such an extent that assignment to a single state is meaningless. The level mixing coefficients for both VPT2+K and HCAO+IU methods are given in the Supporting Information in Tables S11 and S12. The $|0\rangle_f|2\rangle_b$ state is calculated to lie around 100 cm^{-1} lower than the other states with minimal mixing with other states. The energies of this state predicted with the VPT2+K and HCAO+IU methods vary by 48 cm^{-1} and the intensity is 60% larger in the VPT2 calculation. The K and IU corrections have little effect on this state. Despite $|0\rangle_f|1\rangle_b$ being the strongest fundamental transition the corresponding first overtone transition, $|0\rangle_f|2\rangle_b$, is relatively weak in this manifold.[5,61,64]

For the $|20\rangle_+$ state, we find some mixing with the $|11\rangle$ state in the HCAO+IU results, whereas in the VPT2 calculation this state is rather pure. The calculated intensities differ by around an order of magnitude. This state is significantly affected by the K and IU corrections.

In Table 11, we have labeled states that show significant mixing with an asterisk. We have designated these states by the label of the state that has the highest weighting although these assignments should be regarded with caution. Both methods calculate three heavily mixed states in the 7150−7350 cm^{-1} region to consist of transitions to the $|20\rangle_+$, $|2\rangle_f|0\rangle_b$, $|0\rangle_f|1\rangle_b|10\rangle_+$, and $|1\rangle_f|1\rangle_b$ states. We find that the separation of the two lowest energy states in the HCAO+IU method is only 3 cm^{-1}. This is similar to what is predicted using the uncorrected VPT2 method; however, the Darling−Dennsion correction works to lift this degeneracy to a separation of around 75 cm^{-1}. This illustrates the possibilities of large couplings in the normal mode model. The calculated total intensity in this region is similar with the two methods, although it is distributed differently. The state predicted to lie at 7311 cm^{-1} using the VPT2+K method has an intensity of less than 1×10^{-9} in contrast with the corresponding state at 7351 cm^{-1} calculated with the HCAO+IU method with an intensity of 6.3×10^{-8}.

The two highest energy a' states can be assigned to the $|11\rangle$ and $|1\rangle_f|0\rangle_b|10\rangle_+$ states. Interestingly, there is good agreement in the positions and reasonable agreement in the intensity between the two methods although the dominant state in each

case is different. Again, we note that assignment is difficult as there is a high degree of mixing, especially with the VPT2+K method.

We compare our calculated results with the experimental data from the jet-cooled experiment[14] with reference to the Ne matrix isolation data.[17] The bands in the jet-cooled experiment (7 K) are better resolved compared with other experimental data and one band shows rotational structure. In the action spectrum obtained between 7180 and 7300 cm^{-1} four peaks attributed to water dimer are reported. For the first band, lying at 7193 cm^{-1}, a partially resolved rotational structure is observed, which is consistent with an a-type transition, due to the lack of a strong Q-branch. This transition likely corresponds to the band at 7207 cm^{-1} in the Ne matrix isolation spectrum, although the matrix usually lowers the frequency. This rules out assignment to the $|20\rangle_-$ state due to the transition moment of this mode being mostly c-type and as such should exhibit a Q-branch. Simulations of this band suggested an overlapping of two a-type transitions, which were tentatively assigned to the $|20\rangle_+$ or $|1\rangle_f|1\rangle_b$ transitions.[14]

From the HCAO+IU calculation, we see that the $|20\rangle_+$ state lies at 7199 cm^{-1} with a strong intensity and as such is a likely candidate for this assignment. In the VPT2+K calculation the transition at 7162 cm^{-1} is strong and being a combination of mainly the $|20\rangle_+$ and $|2\rangle_f|0\rangle_b$ states also a possible candidate.

Two bands are observed at 7240 and 7249.8 cm^{-1}. These were assigned to the $|2\rangle_f|0\rangle_b$ state, based on previous matrix isolation data which report the bands at 7237 and 7245 cm^{-1}, respectively. The 7237 cm^{-1} band is the dominant band in the matrix isolation spectra. These bands exhibit the perpendicular band shape which would be consistent with a c-type transition and are both quite strong. As previously mentioned, both calculations predict the $|20\rangle_-$ state to be the strongest transition in this region. Hence we assign the $|20\rangle_-$ state to at least one of the bands around 7240 cm^{-1}. The HCAO+IU calculation also predicts a strong transition at 7228 cm^{-1}. This is assigned to the $|2\rangle_f|0\rangle_b$ transition and as such would have a perpendicular band shape so could also be responsible for the bands observed around 7240 cm^{-1}.

The final band observed in the action spectrum is at 7282 cm^{-1} and is not observed in the matrix isolation spectra. This seems to be slightly weaker than the other three bands observed and with a parallel band shape. The parallel band shape could suggest a transition dominated by the $|1\rangle_f|1\rangle_b$ state. The VPT2+K method predicts a band at 7236 cm^{-1}, which is largely made up of the $|0\rangle_f|1\rangle_b|10\rangle_+$ and $|1\rangle_f|1\rangle_b$ states. It has also a rather strong intensity, making this a possibility for assignment to one of the observed bands. The HCAO+IU calculation predicts a similar band at 7225 cm^{-1}, which is largely made up of the $|0\rangle_f|1\rangle_b|10\rangle_+$ state with some contribution from the $|20\rangle_+$ state. This would have the correct symmetry and strong intensity to be assigned to the band observed at 7282 cm^{-1}. However, we also note that the $|1\rangle_f|1\rangle_b$ transition lying at higher energy than the band observed has a similar intensity, thus is also a possible candidate. Because of these all being valid possibilities, we refrain from making any definite assignment to the band observed at 7282 cm^{-1}. The band at 7362 cm^{-1} only observed in the Ne matrix isolation experiment is likely the 7351 cm^{-1} transition in the HCAO+IU calculation or the 7311 cm^{-1} transition in the VPT2+K calculation.

We have also used the ANO basis set together with the VPT2+K and HCAO+IU methods in the hope of resolving some of the remaining ambiguities in assignment in the first OH-stretching overtone region. The mixing coefficients, energies, and intensities of the ten states in the $v_{OH} = 2$ manifold are given in the Supporting Information. For all states, there is a systematic increase in the energies of around 40 cm^{-1} when using the ANO basis set compared to results obtained with the aug-cc-pVTZ basis set. It is interesting that the VPT2/ANO results are closer to the HCAO+IU/aug-cc-pVTZ results, than when comparing same basis set calculations. The intensities from the VPT2 calculation seem more sensitive to basis set than those from the HCAO+IU calculation.

The ANO results seem to be in better agreement with experiment for both vibrational methods. Most of the states exhibit a similar degree of mixing with the slight exception of the VPT2 transition at 7162 cm^{-1} (aug-cc-pVTZ). With the aug-cc-pVTZ basis set, this state is found to consist of an almost equal mixture of $|20\rangle_+$ and $|2\rangle_f|0\rangle_b$, whereas there is a larger component of the $|2\rangle_f|0\rangle_b$ state using the ANO basis. With the ANO basis, this transition is predicted at 7207 cm^{-1} in very good agreement with the observed band at 7193 cm^{-1}. This transition has a large component of $|2\rangle_f|0\rangle_b$ which, as mentioned previously, is expected to lead to an incorrect band shape compare to that observed. Therefore, the HCAO+IU calculations would suggest an assignment of $|20\rangle_+$, and the VPT2+K calculations would suggest the $|2\rangle_f|0\rangle_b$ state mixed with the $|20\rangle_+$ state. Clearly, additional experimental and theoretical work is desirable.

The inclusion of Darling−Dennsion correction to the VPT2 calculation and inclusion of interunit coupling in the HCAO calculations shows that the first OH-stretching overtone of water is indeed very complicated, with most transitions being combinations of many states, making simple one basis state assignment difficult. We find that the inclusion of Darling−Dennison correction to the VPT2 calculations is important to describe the transitions in this region. Inclusion of the interunit coupling in the HCAO model does not significantly alter the energies and intensities of the dominant transitions. This highlights the fundamental difference between the NM and LM approaches.

Conclusion

We have calculated frequencies and intensities of transitions up to ~11 000 cm^{-1} in water and ~8000 cm^{-1} in water dimer. We have compared the results obtained using VPT2, VSCF including cc-VSCF, and a HCAO local mode model. Overall, reasonable agreement with experiment is obtained with all vibrational methods, which all represent significant improvement over the double harmonic approach.

The VSCF and cc-VSCF methods seem to perform well for the OH stretches but are inapplicable for some of the transitions such as the intermolecular vibrational modes. Furthermore, where degeneracies are suspected to be important VSCF is actually preferable to cc-VSCF, because the latter use nondegenerate perturbation theory. For such systems, a degenerate extension to VSCF is required. The HCAO method performs well for the OH-stretching transitions but has problems with transitions to states that involve the HOH-bending modes. This could be aleviated by improving the coupling in the HCAO model to anharmonic coupling. The VPT2 method seems to work well for most transitions. As the energy increases, its accuracy decreases, and for the highest energy OH-stretching transitions the HCAO method provides a suitable alternative. The only method applicable to the intermolecular modes is VPT2, as the HCAO model does not include these six modes and the VSCF model used in this study is inappropriate for such modes. We find that the six low-frequency vibrations do not

have a large effect on the intensity of the dominant OH-stretching and stretch−bend transitions.

For water, we find that the HCAO local mode model is the most accurate in predicting energies and intensities of the OH-stretching modes and that the normal mode models (VPT2, VSCF and cc-VSCF) are better suited to the bending modes. Intensities obtained with the VPT2 and HCAO methods are comparable and agree with experiment to within a factor of 2 for most transitions.

Largely the trends observed for water are observed also for water dimer although it is a much more complicated system. We have investigated the use of additional corrections in the first overtone region to account for Darling−Dennison resonance missing in the VPT2 method and interunit coupling missing in the HCAO method. We find that most transitions in the first OH-stretching overtone region are strongly mixed. For some transitions, we find a significant difference when the Darling−Dennsion corrections are included in VPT2, whereas inclusion of interunit coupling has little effect on the HCAO transitions located on a single water unit. We are able to tentatively assign two of the four peaks recently observed in a jet-cooled action spectrum and offer suggestions for the origin of the remaining two.

The ANO and aug-cc-pVTZ basis sets lead to similar results. In comparison to experimental data for water dimer, the ANO basis set combined with the VPT2 method and the aug-cc-pVTZ basis set combined with the HCAO method give the best agreement.

Acknowledgment. We would like to thank T. W. Robinson and B. J. Miller for helpful discussions. The Marsden Fund administrated by the Royal Society of New Zealand, the Lundbeck Foundation, the U.S. Department of Energy and the Robert A. Welch Foundation have provided funding for this research. H.G.K. is grateful to Aarhus University Research Foundation for a visiting professorship.

Supporting Information Available: The optimized geometries of water and water dimer in Z-matrix format. The calculated local mode parameters of water and water dimer. Full detail of the ANO basis set used in GENBAS format. The calculated energies and intensities of transition in water dimer, using the CCSD(T)/ANO method. The transition energies and intensities of OH-stretching transitions in water dimer, calculated using various HCAO models. The calculated level mixing and eigenvalues for transitions in the first OH-stretching overtone region, calculated using the VPT2+K and HCAO+IU methods. A full list of energies and intensities of transitions calculated using the VPT2, VSCF, and cc-VSCF methods. This material is available free of charge via the Internet at http://pubs.acs.org.

References and Notes

(1) Aloisio, S.; Francisco, J. S. *Acc. Chem. Res.* **2000**, *33*, 825−830.
(2) Vaida, V.; Kjaergaard, H. G.; Feierabend, K. J. *Int. Rev. Phys. Chem.* **2003**, *22*, 203−219.
(3) Hansen, J. C.; Francisco, J. S. *Chem. Phys. Chem.* **2002**, *3*, 833−840.
(4) Huisken, F.; Kaloudis, M.; Kulcke, A. *J. Chem. Phys.* **1996**, *104*, 17−25.
(5) Low, G. R.; Kjaergaard, H. G. *J. Chem. Phys.* **1999**, *110*, 9104−9115.
(6) Morokuma, K.; Muguruma, C. *J. Am. Chem. Soc.* **1994**, *116*, 10316−10317.
(7) Vaida, V.; Daniel, J. S.; Kjaergaard, H. G.; Goss, L. M.; Tuck, A. F. *Q. J. R. Meteorol. Soc.* **2001**, *127*, 1627−1643.
(8) Kjaergaard, H. G.; Robinson, T. W.; Howard, D. L.; Daniel, J. S.; Headrick, J. E.; Vaida, V. *J. Phys. Chem. A* **2003**, *107*, 10680−10686.
(9) Daniel, J. S.; Solomon, S.; Kjaergaard, H. G.; Schofield, D. P. *Geophys. Res. Lett.* **2004**, *31*, L06118.
(10) Ptashnik, I. V.; Smith, K. M.; Shine, K. P.; Newnham, D. A. *Q. J. R. Meteorol. Soc.* **2004**, *130*, 2391−2408.
(11) Huang, Z. S.; Miller, R. E. *J. Chem. Phys.* **1989**, *91*, 6613−6631.
(12) Paul, J. B.; Provencal, R. A.; Chapo, C.; Roth, K.; Casaes, R.; Saykally, R. J. *J. Phys. Chem. A* **1999**, *103*, 2972−2974.
(13) Fredin, L.; Nelander, B.; Ribbegard, G. *J. Chem. Phys.* **1977**, *66*, 4065−4072.
(14) Nizkorodov, S. A.; Ziemkiewicz, M.; Nesbitt, D. J.; Knight, A. E. Q. *J. Chem. Phys.* **2005**, *122*, 194316.
(15) Perchard, J. P. *Chem. Phys.* **2001**, *266*, 109−124.
(16) Perchard, J. P. *Chem. Phys.* **2001**, *273*, 217−233.
(17) Bouteiller, Y.; Perchard, J. P. *Chem. Phys.* **2004**, *305*, 1−12.
(18) Slipchenko, M. N.; Kuyanov, K. E.; Sartakov, B. G.; Vilesov, A. F. *J. Chem. Phys.* **2006**, *124*, 241101 and private communication.
(19) Goss, L. M.; Sharpe, S. W.; Blake, T. A.; Vaida, V.; Brault, J. W. *J. Phys. Chem. A.* **1999**, *103*, 8620−8624.
(20) Paynter, D.; Ptashnik, I.; Shine, K.; Smith, K. *Geophys. Res. Lett.* **2007**, *34*, L12808.
(21) Pfeilsticker, K.; Lotter, A.; Peters, C.; Bösch, H. *Science* **2003**, *300*, 2078−2080.
(22) Suhm, M. A. *Science* **2004**, *304*, 823−824.
(23) Pfeilsticker, K. A. *Science* **2004**, *304*, 824.
(24) Kassi, S.; Macko, P.; Naumenko, O.; Campargue, A. *Phys. Chem. Chem. Phys.* **2005**, *7*, 2460−2467.
(25) Keutsch, F. N.; Braly, L. B.; Brown, M. G.; Harker, H. A.; Petersen, P. B.; Leforestier, C.; Saykally, R. J. *J. Chem. Phys.* **2003**, *119*, 8927−8937.
(26) Leforestier, C.; Gatti, F.; Fellers, R. S.; Saykally, R. J. *J. Chem. Phys.* **2002**, *117*, 8710−8722.
(27) Goldman, N.; Fellers, R. S.; Brown, M. G.; Braly, L. B.; Keoshian, C. J.; Leforestier, C.; Saykally, R. J. *J. Chem. Phys.* **2002**, *116*, 10148−10163.
(28) Smit, M. J.; Groenenboom, G. C.; Wormer, P. E. S.; Avoird, A. v. d.; Bukowski, R.; Szalewicz, K. *J. Phys. Chem. A* **2001**, *105*, 6212−6225.
(29) Bukowski, R.; Szalewicz, K.; Groenenboom, G. C.; Avoird, A. v. d. *Science* **2007**, *315*, 1249−1252.
(30) Burnham, C. J.; Xantheas, S. S. *J. Chem. Phys.* **2002**, *116*, 5115−5124.
(31) Kim, J.; Lee, J. Y.; Lee, S.; Mhin, B. J.; Kim, K. S. *J. Chem. Phys.* **1995**, *102*, 310−317.
(32) Huang, X.; Braams, B. J.; Bowman, J. M. *J. Phys. Chem. A* **2006**, *110*, 445−451.
(33) Feierabend, K. J.; Havey, D. K.; Varner, M. E.; Stanton, J. F.; Vaida, V. *J. Chem. Phys.* **2006**, *124*, 124323.
(34) Kjaergaard, H. G.; Henry, B. R. *J. Chem. Phys.* **1992**, *96*, 4841−4851.
(35) Kjaergaard, H. G.; Low, G. R.; Robinson, T. W.; Howard, D. L. *J. Phys. Chem. A* **2002**, *106*, 8955−8962.
(36) Kjaergaard, H. G. *J. Phys. Chem. A* **2002**, *106*, 2979−2987.
(37) Kjaergaard, H. G.; Bezar, K. J.; Brooking, K. A. *Mol. Phys.* **1999**, *96*, 1125−1138.
(38) Rong, Z.; Henry, B. R.; Robinson, T. W.; Kjaergaard, H. G. *J. Phys. Chem. A* **2005**, *109*, 1033−1041.
(39) Niefer, B. I.; Kjaergaard, H. G.; Henry, B. R. *J. Chem. Phys.* **1993**, *99*, 5682−5700.
(40) Mills, I. M. In *Modern Spectroscopy: Modern Research*; Rao, K. N., Matthews, C. W., Eds.; Academic Press: New York, 1972; pp 115−140.
(41) Vázquez, J.; Stanton, J. F. *Mol. Phys.* **2006**, *104*, 377−388.
(42) Bowman, J. M. *Acc. Chem. Res.* **1986**, *19*, 202−208.
(43) Ratner, M. A.; Gerber, R. B. *J. Phys. Chem.* **1986**, *90*, 20−30.
(44) Chaban, G. M.; Jung, J.-O.; Gerber, R. B. *J. Chem. Phys.* **1999**, *111*, 1823−1829.
(45) Irle, S.; Bowman, J. M. *J. Chem. Phys.* **2000**, *113*, 8401−8403.
(46) Yagi, K.; Taketsugu, T.; Hirao, K.; Gordon, M. S. *J. Chem. Phys.* **2000**, *113*, 1005−1017.
(47) Gerber, R. B.; Chaban, G. M.; Brauer, B.; Miller, Y. In *Theory and applications of computational chemistry: The first 40 years (A volume of technical and historical perspectives)*; Dykstra, C. E., Frenking, G., Kim, K. S., Scuseria, G. E., Eds.; Elsevier: New York, 2005; p 165.
(48) Christiansen, O. *Phys. Chem. Chem. Phys.* **2007**, *9*, 2942−2953.
(49) Chaban, G. M.; Jung, J.-O.; Gerber, R. B. *J. Phys. Chem. A* **2000**, *104*, 2772−2779.
(50) Chaban, G. M.; Xantheas, S. S.; Gerber, R. B. *J. Phys. Chem. A* **2003**, *107*, 4952−4956.
(51) Chaban, G. M.; Gerber, R. B.; Janda, K. C. *J. Phys. Chem. A* **2001**, *105*, 8323−8332.
(52) Chaban, G. M.; Gerber, R. B. *Spectrochim. Acta A* **2002**, *58*, 887−898.
(53) Miller, Y.; Chaban, G. M.; Gerber, R. B. *Chem. Phys.* **2005**, *313*, 213−224.

(54) Miller, Y.; Chaban, G. M.; Gerber, R. B. *J. Phys. Chem. A* **2005**, *109*, 6565−6574.
(55) Chaban, G. M.; Gerber, R. B. *J. Chem. Phys.* **2001**, *115*, 1340−1348.
(56) Gerber, R. B.; Chaban, G. M.; Gregurick, S. K.; Brauer, B. *Biopolymers* **2003**, *68*, 370−382.
(57) Chaban, G. M. *J. Phys. Chem. A* **2004**, *108*, 4551−4556.
(58) Henry, B. R. *Acc. Chem. Res*. **1987**, *20*, 429−435.
(59) Halonen, L.; Carrington, T., Jr. *J. Chem. Phys.* **1988**, *88*, 4171−4185.
(60) Henry, B. R.; Kjaergaard, H. G. *Can. J. Chem.* **2002**, *80*, 1635−1642.
(61) Schofield, D. P.; Kjaergaard, H. G. *Phys. Chem. Chem. Phys.* **2003**, *5*, 3100−3105.
(62) Kjaergaard, H. G.; Henry, B. R.; Wei, H.; Lefebvre, S.; Carrington, T., Jr.; Mortensen, O. S.; Sage, M. L. *J. Chem. Phys.* **1994**, *100*, 6228−6239.
(63) Rong, Z.; Howard, D. L.; Kjaergaard, H. G. *J. Phys. Chem. A* **2003**, *107*, 4607−4611.
(64) Schofield, D. P.; Lane, J. R.; Kjaergaard, H. G. *J. Phys. Chem. A* **2007**, *111*, 567−572.
(65) Gauss, J.; Stanton, J. F. *Chem. Phys. Lett.* **1997**, *276*, 70−77.
(66) Stanton, J. F.; Lopreore, C. L.; Gauss, J. *J. Chem. Phys.* **1988**, *108*, 7190−7196.
(67) Jung, J.-O.; Gerber, R. B. *J. Chem. Phys.* **1996**, *105*, 10332−10348.
(68) Njegic, B.; Gordon, M. S. *J. Chem. Phys.* **2006**, *125*, 224102.
(69) Matsunaga, N.; Chaban, G. M.; Gerber, R. B. *J. Chem. Phys.* **2002**, *117*, 3541−3547.
(70) Howard, D. L.; Jørgensen, P.; Kjaergaard, H. G. *J. Am. Chem. Soc.* **2005**, *127*, 17096−17103.
(71) Wilson, E. B., Jr.; Decius, J. C.; Cross, P. C. *Molecular Vibrations*; Dover Publications, Inc.: New York, 1980.
(72) Raghavachari, K.; Trucks, G. W.; Pople, J. A.; Head-Gordon, M. *Chem. Phys. Lett.* **1989**, *157*, 479−483.
(73) Bartlett, R. J.; Watts, J. D.; Kucharski, S. A.; Noga, J. *Chem. Phys. Lett.* **1990**, *165*, 513−522.
(74) Dunning, T. H., Jr. *J. Chem. Phys.* **1988**, *90*, 1007−1023.
(75) Almlöf, J.; Taylor, P. R. *J. Chem. Phys.* **1987**, *86*, 4070−4077.
(76) The General Atomic and Molecular Electronic Structure System (GAMESS) a general ab initio quantum chemistry package, www.msg.chem.iastate.edu/gamess/gamess.html.
(77) Schmidt, M. W.; Baldrisge, K. K.; Boatz, J. A.; Elbert, S. T.; Gordon, M. S.; Jensen, J. H.; Koseki, S.; Matsunaga, N.; Nguyen, K. A.; Su, S.; Windus, T. L.; Dupuis, M.; Montgomery, J. A. *J. Comp. Chem.* **1993**, *14*, 1347−1363.
(78) Frisch, M. J.; Trucks, G. W.; Schlegel, H. B.; Scuseria, G. E.; Robb, M. A.; Cheeseman, J. R.; Montgomery, Jr., J. A.; Vreven, T.; Kudin, K. N.; Burant, J. C.; Millam, J. M.; Iyengar, S. S.; Tomasi, J.; Barone, V.; Mennucci, B.; Cossi, M.; Scalmani, G.; Rega, N.; Petersson, G. A.; Nakatsuji, H.; Hada, M.; Ehara, M.; Toyota, K.; Fukuda, R.; Hasegawa, J.; Ishida, M.; Nakajima, T.; Honda, Y.; Kitao, O.; Nakai, H.; Klene, M.; Li, X.; Knox, J. E.; Hratchian, H. P.; Cross, J. B.; Adamo, C.; Jaramillo, J.; Gomperts, R.; Stratmann, R. E.; Yazyev, O.; Austin, A. J.; Cammi, R.; Pomelli, C.; Ochterski, J. W.; Ayala, P. Y.; Morokuma, K.; Voth, G. A.; Salvador, P.; Dannenberg, J. J.; Zakrzewski, V. G.; Dapprich, S.; Daniels, A. D.; Strain, M. C.; Farkas, O.; Malick, D. K.; Rabuck, A. D.; Raghavachari, K.; Foresman, J. B.; Ortiz, J. V.; Cui, Q.; Baboul, A. G.; Clifford, S.; Cioslowski, J.; Stefanov, B. B.; Liu, G.; Liashenko, A.; Piskorz, P.; Komaromi, I.; Martin, R. L.; Fox, D. J.; Keith, T.; Al-Laham, M. A.; Peng, C. Y.; Nanayakkara, A.; Challacombe, M.; Gill, P. M. W.; Johnson, B.; Chen, W.; Wong, M. W.; Gonzalez, C.; Pople, J. A. *Gaussian 03*, revision C.02; Gaussian, Inc.: Wallingford, CT, 2004.
(79) Stanton, J. F.; Gauss, J.; Watts, J. D.; Szalay, P. G. Bartlett, R. J. with contributions from Auer, A. A.; Bernholdt, D. B.; Christiansen, O.; Harding, M. E.; Heckert, M.; Heun, O.; Huber, C.; Jonsson, D.; Jusélius, J.; Lauderdale, W. J.; Metzroth, T.; Michauk, C.; O'Neill, D. P.; Price, D. R.; Ruud, K.; Schiffmann, F.; Tajti, A.; Varner, M. E.; Vázquez, J. and the integral packages MOLECULE (Almlöf J.; Taylor, P. R.), PROPS (Taylor, P. R.), and ABACUS (Helgaker, T.; Aa. Jensen, H. J.; Jørgensen, P.; Olsen, J.). For the current version, see http://www.aces2.de.
(80) Werner, H.-J.; Knowles, P. J.; Lindh, R.; Schütz, M.; Celani, P.; Korona, T.; Manby, F. R.; Rauhut, G.; Amos, R. D.; Bernhardsson, A.; Berning, A.; Cooper, D. L.; Deegan, M. J. O.; Dobbyn, A. J.; Eckert, F.; Hampel, C.; Hetzer, G.; Lloyd, A. W.; McNicholas, S. J.; Meyer, W.; Mura, M. E.; Nicklass, A.; Palmieri, P.; Pitzer, R.; Schumann, U.; Stoll, H.; Stone, A. J.; Tarroni, R.; Thorsteinsson, T. *MOLPRO*, version 2002.6, a package of ab initio programs; 2003.
(81) Dyke, T. R.; Mack, K. M.; Muenter, J. S. *J. Chem. Phys.* **1977**, *66*, 498−510.
(82) There are some minor errors in the equations for the dressed K_{abcd} matrix elements given in ref 88. All of these have been rederived in the course of this research and checked with a numerical (explicit summation) VPT2 program developed and discussed in ref 41. The correct equations will be given elsewhere (Matthews, D. A.; Vázquez, J.; Stanton, J. F. *Mol. Phys.*, in press). Also, Coriolis contributions are included in the present work only within the framework of VPT2; additional contributions from the Coriolis ζ constants have not been included in the K_{abcd} used here.
(83) Salmi, T.; Hänninen, V.; Garden, A. L.; Kjaergaard, H. G.; Tennyson, J.; Halonen, L. *J. Phys. Chem. A*, in press.
(84) Seidler, P.; Kongsted, J.; Christiansen, O. *J. Phys. Chem. A* **2007**, *111*, 11205−11213.
(85) Dyke, T. R.; Muenter, J. S. *J. Chem. Phys.* **1973**, *59*, 3125−3127.
(86) Garden, A. L.; Halonen, L.; Kjaergaard, H. G. Submitted to *J. Phys. Chem. A.*
(87) Darling, B. T.; Dennison, D. M. *Phys. Rev.* **1940**, *57*, 128−139.
(88) Lehmann, K. K. *Mol. Phys.* **1989**, *66*, 1129−1137.
(89) Buck, U.; Huisken, F. *Chem. Rev.* **2000**, *100*, 3863−3890.
(90) Braly, L. B.; Liu, K.; Brown, M. G.; Keutsch, F. N.; Fellers, R. S.; Saykally, R. J. *J. Chem. Phys.* **2000**, *112*, 10314−10326.